


# Dynamically Corrected Nonadiabatic Holonomic Quantum Gates

Sai Li<sup>1</sup> and Zheng-Yuan Xue<sup>1,2,\*</sup>

<sup>1</sup>*Guangdong Provincial Key Laboratory of Quantum Engineering and Quantum Materials, and School of Physics and Telecommunication Engineering, South China Normal University, Guangzhou 510006, China*

<sup>2</sup>*Guangdong-Hong Kong Joint Laboratory of Quantum Matter, and Frontier Research Institute for Physics, South China Normal University, Guangzhou 510006, China*

 (Received 5 January 2021; revised 19 April 2021; accepted 13 September 2021; published 5 October 2021)

The key for realizing fault-tolerant quantum computation lies in maintaining the coherence of all qubits so that high-fidelity and robust quantum manipulations on them can be achieved. One of the promising approaches is to use geometric phases in the construction of universal quantum gates, due to their intrinsic robustness against certain types of local noise. However, due to limitations in previous implementations, the noise-resilience feature of nonadiabatic holonomic quantum computation (NHQC) still needs to be improved. Here, in combination with the dynamical-correction technique, we propose a general protocol of universal NHQC with simplified control, which can greatly suppress the effect of the accompanied  $X$  errors, retaining the main merit of geometric quantum operations. Numerical simulation shows that the performance of our gate can be much better than that of previous protocols. Remarkably, when incorporating a decoherence-free subspace encoding for the collective dephasing noise, our scheme can also be robust against the involved  $Z$  errors. In addition, we also outline the physical implementation of the protocol, which is insensitive to both  $X$  and  $Z$  errors. Therefore, our protocol provides a promising strategy for scalable fault-tolerant quantum computation.

DOI: [10.1103/PhysRevApplied.16.044005](https://doi.org/10.1103/PhysRevApplied.16.044005)

## I. INTRODUCTION

Quantum computation and its physical implementation have attracted much attention following the discovery of Shor's algorithm [1], which is an efficient algorithm for factorizing prime numbers, a hard problem for classical computers. However, up to now, the physical realization of large-scale and fault-tolerant quantum computation [2] has remained challenging due to the inevitable noise and operational errors when manipulating a qubit. Therefore, considering the fact that the coherence time of quantum systems is limited, the attainment of fast and robust quantum gates with high fidelity is the key for realizing large-scale fault-tolerant quantum computation.

Geometric phases [3–5] are induced on a quantum system by moving a set of its Hamiltonian parameters to form a cyclic evolution in the parametric space and are determined by the trajectory that the quantum system travels. This global property leads to the intrinsic noise-resilient feature of geometric phases, which finds promising application in quantum computation, where quantum gates are implemented using geometric phases, i.e., geometric quantum computation [6–9]. Recently, based on fast nonadiabatic non-Abelian geometric phases, quantum computation

protocols have been proposed [10,11] and expanded extensively [12–21], with elementary experimental demonstrations [22–29] on various quantum systems. However, due to the implementation limitations, the preferred merit of being resilient against operational control error, i.e., the  $X$  error, of the geometric phases is compromised [30,31].

Meanwhile, to deal with general errors in nonadiabatic holonomic quantum computation (NHQC), various protocols have also been proposed, with preliminary experimental demonstrations. Specifically, besides the conventional wisdom of using an error-avoiding encoding technique [32–42], which is resource inefficient, incorporation with other control techniques in NHQC has also been introduced, such as the relatively experimentally friendly composite scheme [43,44] or the dynamical decoupling strategy [45,46], the deliberately optimal pulse-control technique [47–52], shortening the gate-time method with prescribed complex pulses [53–57], etc. However, in these previous explorations, the enhancement of the gate robustness has been obtained at the cost of the deliberate pulse-shape control technique and/or has greatly extended the gate time. Thus, the NHQC protocol with simplified control, while retaining the strong gate robustness, is highly desired.

Here, in combination with the dynamical-correction technique [58–60], we propose a general protocol for universal NHQC without deliberate pulse control and with

\*zyxue83@163.com

experimentally accessible techniques, termed as DCN-HQC, which can improve gate robustness against the  $X$  error from the second order in the conventional NHQC case to the fourth order, thus retaining the main merit of geometric quantum gates. Our gate time is the same as that of the two-loop composite NHQC (CNHQC) scheme [44], which is much shorter than the NHQC with optimal control (NHQCOC) scheme [49,50]. However, numerical simulation shows that the gate robustness in our scheme can be much better than that of both the conventional single-loop NHQC [15] and the CNHQC. Due to the longer gate time, the gate infidelity of NHQCOC is much higher than the current scheme, although they share similar gate-robustness performance. Meanwhile, our scheme can be incorporated with a decoherence-free subspace (DFS) encoding for the collective dephasing noise [61–63], which is robust against the collective  $Z$  error. In this way, the present protocol can be immune to both  $X$  and  $Z$  errors. Note that the origin of the gate-robustness enhancement here is different from Ref. [64]. The enhancement there is due to the much shorter gate time and thus the decoherence and errors can only affect the quantum dynamics in a shorter time span. Here, the robustness of the current scheme is stronger than in Ref. [64] but the gate fidelity here is lower, due to the longer gate time. Finally, we outline the physical implementation of the protocol, which is insensitive to both  $X$  and  $Z$  errors, with conventional exchange interactions among physical qubits, where the unwanted leakage errors can be effectively eliminated. Therefore, our protocol provides a promising strategy toward large-scale fault-tolerant quantum computation.

## II. CONVENTIONAL HOLONOMIC GATES

First, we summarize the realization of the conventional single-loop NHQC [13–15], which is an efficient extension of the original NHQC proposal [10,11]. We consider a three-level quantum system that is resonantly driven by two different external pulses with amplitude envelopes  $\Omega_0(t)$  and  $\Omega_1(t)$  and initial phases  $\phi_0$  and  $\phi_1$ , respectively. In the interaction picture, setting  $\hbar = 1$  hereafter, the interaction Hamiltonian of the driving quantum system is

$$\begin{aligned} \mathcal{H}(t) &= [\Omega_0(t)e^{-i\phi_0}|0\rangle + \Omega_1(t)e^{-i\phi_1}|1\rangle] \langle a| + \text{H.c.} \\ &= \Omega(t)e^{-i\phi_0}|b\rangle \langle a| + \text{H.c.}, \end{aligned} \quad (1)$$

where  $\{|0\rangle, |1\rangle\}$  is our chosen computational basis, i.e., the two qubit states, and  $|a\rangle$  is an auxiliary state;  $\Omega(t) = \sqrt{\Omega_0^2(t) + \Omega_1^2(t)}$ ,  $|b\rangle = \sin(\theta/2)|0\rangle - \cos(\theta/2)e^{i\phi}|1\rangle$  with  $\phi = \phi_0 - \phi_1 + \pi$ , and  $\tan(\theta/2) = \Omega_0(t)/\Omega_1(t)$ , where  $\theta$  is a constant angle; and  $(\theta, \phi)$  determine the rotation axis of the implemented gates, as illustrated later. This interacting Hamiltonian has a dark state of  $|d\rangle = -\cos(\theta/2)e^{-i\phi}|0\rangle -$

$\sin(\theta/2)|1\rangle$ , which is decoupled from the other eigenstates during the quantum dynamics.

With the above Hamiltonian, conventional NHQC can be realized in a single-loop way and in the dressed basis  $\{|b\rangle, |d\rangle\}$ , the cyclic evolution path is shown in Fig. 1(a) and with  $\gamma_g = \pi/2$ . Specifically, for the first half of the evolution, i.e.,  $t \in [0, T/2]$  where  $T$  is the whole gate time, under the Hamiltonian in Eq. (1) with  $\int_0^{T/2} \Omega(t)dt = \pi/2$ , the bright state  $|b\rangle$  starts from the northern pole and travels down to the southern pole along the line of longitude determined by  $\phi_0$ , where it is clockwise rotated through an angle  $\gamma_g$ . Then, it goes back to the northern pole, also along a line of longitude, determined by  $\phi_0 + \pi - \gamma_g$  under the Hamiltonian in Eq. (1), with  $\int_{T/2}^T \Omega(t)dt = \pi/2$ . After this cyclic evolution, with a total  $\pi$  pulse, the  $|b\rangle$  state acquires a pure geometric phase  $\gamma_g$ , while  $|d\rangle$  is not changed, and thus the corresponding holonomic quantum gate operation is

$$U = |d\rangle \langle d| + e^{i\gamma_g}|b\rangle \langle b|. \quad (2)$$

Notably, the  $|a\rangle$  state is not our computational state and its population stays unchanged before and after the gate operation; thus we do not include this component in the above equation. Correspondingly, in the computational basis of  $\{|0\rangle, |1\rangle\}$ , the holonomic gate in Eq. (2) is

$$U = e^{i\frac{\gamma_g}{2}} e^{-i\frac{\gamma_g}{2} \mathbf{n} \cdot \boldsymbol{\sigma}}, \quad (3)$$

where  $\mathbf{n} = (\sin \theta \cos \phi, -\sin \theta \sin \phi, \cos \theta)$  and  $\boldsymbol{\sigma} = (\sigma_x, \sigma_y, \sigma_z)$ , with  $\sigma_{x,y,z}$ , are Pauli matrices in the computational basis. This operation denotes a rotation along the  $\mathbf{n}$  axis through an angle of  $\gamma_g$ . As  $\mathbf{n}$  and  $\gamma_g$  can be arbitrary, universal single-qubit quantum gates are constructed.

However, as shown in Fig. 1(b), this type of implementation is not robust against the  $X$  error. In the presence of the  $X$  error, i.e.,  $\mathcal{H}^\epsilon(t) = (1 + \epsilon)\mathcal{H}(t)$ , where  $\epsilon$  is the deviation fraction of the amplitude of the driving fields, the evolution can be solved by  $U^\epsilon(t) = e^{-i\mathcal{H}^\epsilon(t)t}$ . Then, the implemented holonomic gate in the dressed basis  $\{|b\rangle, |d\rangle\}$  changes to

$$U^\epsilon = |d\rangle \langle d| + \left( \cos^2 \frac{\mu\pi}{2} + \sin^2 \frac{\mu\pi}{2} e^{i\gamma_g} \right) |b\rangle \langle b|, \quad (4)$$

where  $\mu = 1 + \epsilon$ . Thus, when the  $X$  error is small, i.e.,  $\epsilon \ll 1$ , the gate fidelity in the dressed basis  $\{|b\rangle, |d\rangle\}$  decreases from perfect unity to

$$\begin{aligned} F &= \frac{|\text{Tr}(U^\dagger U^\epsilon)|}{|\text{Tr}(U^\dagger U)|} = \frac{1}{2} \left| 1 + \cos^2 \frac{\mu\pi}{2} e^{-i\gamma_g} + \sin^2 \frac{\mu\pi}{2} \right| \\ &\approx 1 - \epsilon^2 \pi^2 (1 - \cos \gamma_g)/8, \end{aligned} \quad (5)$$

which shows that the holonomic quantum gates in the conventional single-loop NHQC scheme can only suppress the

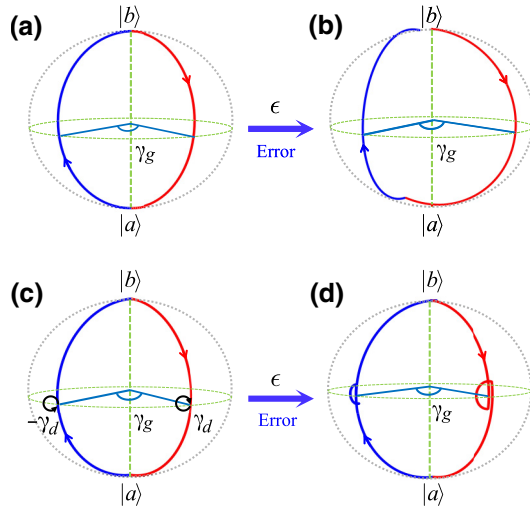


FIG. 1. A schematic illustration of the evolution paths for holonomic quantum gates in Eq. (3) with  $\gamma_g = \pi/2$ . The evolution paths of the bright state  $|b\rangle$  for the conventional NHQC scheme (a) without and (b) with the systematic  $X$  error, which obviously leads to the gate error. The evolution paths of the bright state  $|b\rangle$  in the DCNHQC scheme (c) without and (d) with the  $X$  error. As shown in (d), the  $X$  error can be efficiently eliminated by the dynamical-correction process.

$X$  error up to the second order, similar to the performance of dynamical quantum gates [30,31]. In this way, when the quantum system suffers from systematic  $X$  errors, the  $|b\rangle$  state cannot exactly go back to the original starting point after the designed cyclic evolution, as shown in Fig. 1(b), and thus leads to infidelity of the implemented quantum gate.

### III. DYNAMICALLY CORRECTED HOLONOMIC GATES

We now turn to the implementation of the dynamically corrected holonomic gates. To reduce the influence of the  $X$  error in conventional NHQC, under the guidance of the dynamical-correction technique [58–60], we insert two dynamical processes to enhance the robustness against the  $X$  error in conventional NHQC. Notably, this dynamical correction also works when the two inserted dynamical processes also have  $X$  errors. First, as shown in Fig. 1(c), we consider the ideal case to explain the evolution process, where the two dynamical processes are, respectively, inserted at the midpoint in each half of the evolution path. In this way, although there are dynamical phases that accumulate during each dynamical processes, their summation is zero, leaving a pure geometric phase  $\gamma_g$  on the dressed state  $|b\rangle$ , and thus the whole process can still lead to universal single-qubit holonomic gates in Eq. (3).

Specifically, at the midpoint of the first half of the evolution path, i.e., at the time  $T/4$ , a Hamiltonian

$$\mathcal{H}_1^I(t) = \Omega_1^I(t) e^{-i(\phi_0 + \pi/2)} |b\rangle\langle a| + \text{H.c.} \quad (6)$$

with  $\int_{T/4}^{3T/4} \Omega_1^I(t) dt = \pi/2$  is inserted. Due to this inserted pulse, the starting time of the second half of the evolution path changes to  $T$  and a second inserted Hamiltonian

$$\mathcal{H}_2^I(t) = \Omega_2^I(t) e^{-i(\phi_0 - \gamma_g - \pi/2)} |b\rangle\langle a| + \text{H.c.}, \quad (7)$$

with  $\int_{5T/4}^{7T/4} \Omega_2^I(t) dt = \pi/2$ , is turned on at the time  $5T/4$ . Therefore, in this case, the total gate time is  $2T$  and the total pulse area is  $2\pi$ . Nevertheless, there is still no specific restriction on the shapes of  $\Omega(t)$ ,  $\Omega_1^I(t)$ , and  $\Omega_2^I(t)$ , except for their integration. In this way, even in the presence of the  $X$  error during the whole evolution process, including in both the conventional NHQC process and the two inserted dynamical processes, the dressed state  $|b\rangle$  can still go back to the original starting point after the cyclic evolution with high accuracy, as shown in Fig. 1(d), leading to robust holonomic quantum gates.

We next proceed to analytically prove the above result. In the presence of the  $X$  error, including in both the conventional NHQC process and the two inserted dynamical processes, the error Hamiltonian is  $\mathcal{H}^\epsilon(t)$  as defined before and the holonomic gates in the dressed basis  $\{|b\rangle, |d\rangle\}$  change to

$$U_c^\epsilon = \left[ \cos^4 \frac{\mu\pi}{2} + \left( \sin^2 \frac{\mu\pi}{2} + \frac{1}{4} \sin^2 \mu\pi \right) e^{i\gamma_g} \right] |b\rangle\langle b| + |d\rangle\langle d|. \quad (8)$$

Then, when the  $X$  error is small, i.e.,  $\epsilon \ll 1$ , the gate fidelity in the dressed basis  $\{|b\rangle, |d\rangle\}$  of the three-level quantum system is

$$\begin{aligned} F_c &= \frac{|\text{Tr}(U^\dagger U_c^\epsilon)|}{|\text{Tr}(U^\dagger U)|} \\ &= \frac{1}{2} \left| 1 + \sin^2 \frac{\mu\pi}{2} + \frac{1}{4} \sin^2 \mu\pi + \cos^4 \frac{\mu\pi}{2} e^{-i\gamma_g} \right| \\ &\approx 1 - \epsilon^4 \pi^4 (1 - \cos \gamma_g) / 32, \end{aligned} \quad (9)$$

which shows that dynamically corrected holonomic gates can improve the gate robustness against the  $X$  error from the second order in the conventional NHQC case (see Eq. (5)) to the fourth order. As shown in Fig. 1(d), in this case—the geometric trajectory starting from the dressed state  $|b\rangle$ —the evolution process is driven by  $\mathcal{H}^\epsilon(t)$  with  $X$  errors; however, by inserting two dynamically corrected Hamiltonians, which also be with the  $X$  error, the compromised evolution process is now corrected. That is to say,

the dressed state  $|b\rangle$  arrives at the dressed basis  $|a\rangle$  accurately after the first half of the evolution path, and then goes back to the dressed basis  $|b\rangle$  accurately during the second half, and finally acquires a pure geometric phase.

Furthermore, to faithfully confirm our results, we consider a V-type three-level quantum system as shown in Fig. 2(a) to simulate the gate performance of the proposed single-qubit gates using the Lindblad master equation

$$\dot{\rho}_1 = i[\rho_1, \mathcal{H}] + \frac{1}{2} \sum_{n=1}^4 \Gamma_n \mathcal{L}(\sigma_n), \quad (10)$$

where  $\rho_1$  is the density matrix of the system under consideration and  $\mathcal{L}(\sigma_n) = 2\sigma_n \rho_1 \sigma_n^\dagger - \sigma_n^\dagger \sigma_n \rho_1 - \rho_1 \sigma_n^\dagger \sigma_n$  is the Lindbladian of the operator  $\sigma_n$ , with  $\sigma_1 = |a\rangle\langle 0|$ ,  $\sigma_2 = |a\rangle\langle 1|$ ,  $\sigma_3 = (|0\rangle\langle 0| - |a\rangle\langle a|)/2$ ,  $\sigma_4 = (|1\rangle\langle 1| - |a\rangle\langle a|)/2$ , and  $\Gamma_n$  as their corresponding decoherence rates. For typical systems that are suitable for physical implementation of quantum computation, the  $\Gamma_n/\Omega_m$  ratio with  $\Omega_m = \max\{\Omega(t)\}$  can be well below the  $10^{-4}$  value within current state-of-art technologies, even for the solid-state quantum systems, which typically have shorter coherence times. For example, for superconducting transmon qubits [2,65], the qubit coherence time can approach 0.1 ms, corresponding to a kilohertz-level decoherence rate, while the Rabi frequency can be tens of megahertz. In our simulation, we set  $\Omega(t) = \Omega_m = 1$ ,  $\phi_0(0) = 0$  and the decoherence rates  $\Gamma_n = \Gamma = 5 \times 10^{-4}$ . Specifically, we numerically demonstrate the state population and fidelity dynamics of the dynamically corrected Hadamard ( $H$ ) gate with  $\theta = \pi/4$ ,  $\gamma_g = \pi$ ,  $\phi = 0$  and  $S$  gate with  $\theta = 0$ ,  $\gamma_g = \pi/2$ ,  $\phi = 0$ . The corresponding initial states are set to be  $|\psi_i\rangle_H = |0\rangle$  and  $|\psi_i\rangle_S = (|0\rangle + |1\rangle)/\sqrt{2}$ , respectively. Furthermore, we use the state fidelities, defined by  $F_{H/S} = \langle \psi_f | \rho_1 | \psi_f \rangle_{H/S}$ , where  $|\psi_f\rangle_H = (|0\rangle + |1\rangle)/\sqrt{2}$  and  $|\psi_f\rangle_S = (|0\rangle + i|1\rangle)/\sqrt{2}$  are the corresponding ideal target states, to evaluate these two gates. As shown in Figs. 3(a) and 3(b), we obtain the state fidelities for the  $H$  and  $S$  gates as  $F_H = 99.69\%$  and  $F_S = 99.73\%$ , respectively. The amplitude envelopes of  $\Omega(t)$  and the phase envelopes of  $\phi_0$  of the Hamiltonian  $\mathcal{H}(t)$  for  $S$  gate are plotted in Fig. 3(c). Besides, to fully evaluate the gate performance, using six initial states  $|0\rangle, |1\rangle, (|0\rangle + |1\rangle)/\sqrt{2}, (|0\rangle - |1\rangle)/\sqrt{2}, (|0\rangle + i|1\rangle)/\sqrt{2}$ , and  $(|0\rangle - i|1\rangle)/\sqrt{2}$ , we define the gate fidelity as [66]

$$F_1^G = \frac{1}{6} \sum_{j=1}^6 \langle \psi_j | U^\dagger \rho_1 U | \psi_j \rangle. \quad (11)$$

The gate fidelities of the  $H$  and  $S$  gates are  $F_H^G = 99.74\%$  and  $F_S^G = 99.74\%$ , respectively, and the infidelity is mainly due to the decoherence effect. Furthermore, we

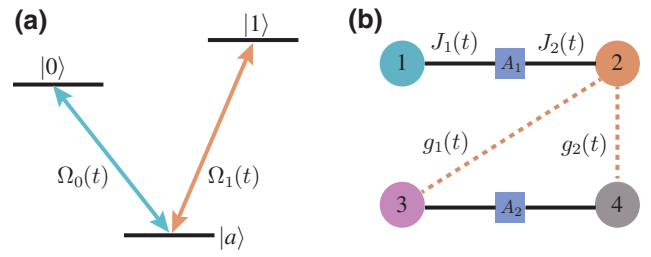


FIG. 2. The setup of our proposal. (a) A V-type three-level system with resonantly driving  $|0\rangle \leftrightarrow |a\rangle$  and  $|1\rangle \leftrightarrow |a\rangle$  transitions. (b) The coupling configuration for a nontrivial two-qubit holonomic quantum gate. The circles with different colors denote the physical qubits with different frequencies, the squares denote auxiliary physical qubits, and the black solid and orange dashed bonds indicate that the interactions are for single- and two-qubit gates, respectively.

numerically confirm that when  $\Gamma \leq 2 \times 10^{-4}$ , both gate fidelities can exceed 99.9%.

Finally, to demonstrate the robustness of the dynamically corrected holonomic gates, we consider the  $X$  error within the range of  $-0.1 \leq \epsilon \leq 0.1$ , and select the  $S$  gate for demonstration purposes. First, in the case without decoherence, we numerically compare the robustness of the present DCNHQC, the conventional single-loop NHQC [15], the two-loop CNHQC [44], and the NHQCOC [49,50] cases. As shown in Fig. 3(d), both DCNHQC and NHQCOC can improve the gate robustness against the  $X$  error from the second order in the conventional

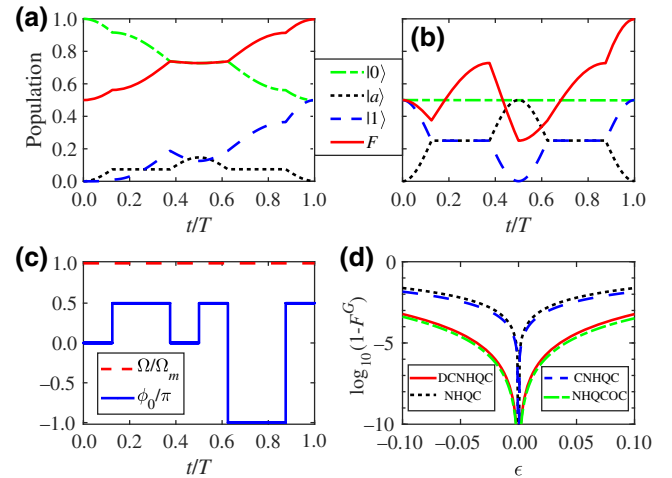


FIG. 3. The state population and fidelity dynamics for the dynamically corrected holonomic (a)  $H$  and (b)  $S$  gates. (c) The shapes of the  $\Omega$  and phases  $\phi_0$  in  $\mathcal{H}(t)$  for the  $S$  gate. (d) The gate robustness with the logarithm to base ten of the gate infidelity for the  $S$  gate under the  $X$  error without decoherence, obtained from DCNHQC, NHQCOC, conventional single-loop NHQC, and two-loop CNHQC, where the first two techniques show better performance.

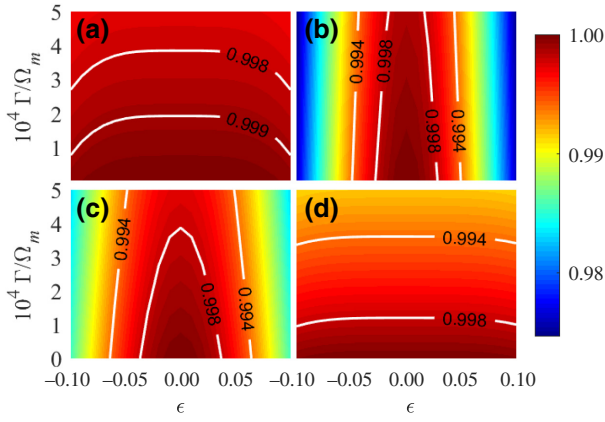


FIG. 4. The robustness of the  $S$  gate in the (a) DCNHQC, (b) conventional single-loop NHQC, (c) two-loop CNHQC, and (d) NHQCOC cases, considering both the  $X$  error and the decoherence effect with a uniform decoherence rate  $\Gamma/\Omega_m$ . In this realistic case, the proposed DCNHQC strategy performs best.

NHQC case to the fourth order, which demonstrates the stronger robustness of dynamically corrected holonomic gates against the  $X$  error. Second, we repeat the above comparison under decoherence, with a uniform rate of  $\Gamma_n = \Gamma \in [0, 5] \times 10^{-4}$ . As shown in Fig. 4, after considering the influence of both the  $X$  error and the decoherence effect, the current DCNHQC protocol performs best. In this case, the gate fidelity in the NHQCOC case decreases rapidly, as it suffers severely from the decoherence effect, due to the longer gate time required by deliberately engineered pulse shapes. In addition, from Fig. 4(a), when  $\Gamma \leq 0.9 \times 10^{-4}$ , the fidelity for all gates can be higher than 99.9% for the  $X$  error within the range of  $-0.1 \leq \epsilon \leq 0.1$ . Thus, our proposal is apparently more robust than previous ones.

#### IV. PHYSICAL IMPLEMENTATION

In this last section, we show that, based on the dynamically corrected technique, the  $X$  error can be suppressed well for dynamically corrected holonomic gates. Meanwhile, when incorporating a DFS encoding for the collective dephasing noise, our scheme can also be robust against the collective  $Z$  error. We now turn to consider the physical implementation of the scheme combining the dynamically correction technique and the DFS encoding. We consider three resonantly coupled two-level qubits with conventional two-body exchange interaction as shown in Fig. 2(b), the Hamiltonian of which is

$$\mathcal{H}_1(t) = J_1(t)e^{-i\varphi_1}S_1^+S_{A_1}^- + J_2(t)e^{-i\varphi_2}S_2^+S_{A_1}^- + \text{H.c.}, \quad (12)$$

where  $J_k(t)$  ( $k = 1, 2$ ) are coupling strengths between qubits  $Q_k$  and  $Q_{A_1}$ , and  $S^+ = |1\rangle\langle 0|$  is the creation operator. This exchange-interaction Hamiltonian is very general and can be implemented in trapped ions [34],

cavity-coupled N-V centers [35], different superconducting quantum circuit setups [36–39,41,55], etc. Then, we combine three physical qubits and encode them into a logical qubit that belongs to a three-dimensional DFS  $\mathcal{S}_1 = \text{Span}\{|100\rangle, |010\rangle, |001\rangle\}$ , with  $|100\rangle \equiv |1\rangle_1 \otimes |0\rangle_2 \otimes |0\rangle_{A_1}$ . In this single-excitation subspace, the logical qubit states are defined as  $\{|0\rangle_L = |100\rangle$  and  $|1\rangle_L = |010\rangle\}$ , with  $|A_1\rangle_L = |001\rangle$  serving as an ancillary state. To prepare arbitrary states in logical qubit subspace, we can encode an arbitrary state on physical qubit 1, e.g.,  $|\psi\rangle_1 = a|1\rangle_1 + b|0\rangle_1$ , into the logical qubit subspace, i.e.,  $|\psi\rangle_L = a|100\rangle + b|010\rangle = a|0\rangle_L + b|1\rangle_L$ . When the other two qubits are both in their ground states, this can be achieved as following. First, a NOT gate is applied on qubit 2 and then a controlled-NOT (CNOT) gate is applied on qubits 1 and 2, with qubit 1 being the control qubit. Meanwhile, the decoding circuit can be obtained by inverting these two steps. In the logical basis, Eq. (12) can be rewritten as

$$\mathcal{H}_L^1(t) = J_1(t)e^{-i\varphi_1}|0\rangle_L\langle A_1| + J_2(t)e^{-i\varphi_2}|1\rangle_L\langle A_1| + \text{H.c.}, \quad (13)$$

which has the same form as the Hamiltonian  $\mathcal{H}(t)$  in Eq. (1) and thus can naturally be used to apply the DCNHQC strategy to suppress the  $X$  error. When  $\Gamma = 2 \times 10^{-4}$ , the fidelity of the  $H$  gate is 99.85%, where the infidelity is mainly due to the decoherence effect of the physical qubits.

Here, we also compare the gate robustness of our DCNHQC without and with the DFS encoding in Fig. 5, considering both the  $X$  and  $Z$  errors for  $\mathcal{H}^E(t) = (1 + \epsilon)\mathcal{H}(t) - \delta\Omega_m|a\rangle\langle a|$  and  $\mathcal{H}_L^E(t) = (1 + \epsilon)\mathcal{H}_L^1(t) - \delta\Omega_m(|0\rangle_L\langle 0| + |1\rangle_L\langle 1| + |A_1\rangle_L\langle A_1|)$ , respectively. We consider the  $S$  gate for a typical example. As shown in Fig. 5(a), the gate from DCNHQC can only suppress the  $X$  error, while combining it with the DFS encoding, the gate with encoding can suppress both the  $X$  and  $Z$  errors and the gate infidelities are well within 0.1% in the error range under consideration, as shown in Fig. 5(b). Here, for the numerical simulation of the DFS encoding case, we consider a simple case in which the dephasing is collective, i.e., the  $Z$  error is the same for each physical qubit. When the  $Z$  errors  $\delta_j$  are different in physical qubits, the DFS encoding can still eliminate the overlapping part of the  $\delta_j$  drifts, which are of low-frequency nature for solid-state qubits and thus can be regarded as constants during a certain quantum gate operation.

In addition, to realize universal quantum computation, a nontrivial two-qubit gate is also necessary. Next, we consider six two-level physical qubit systems with effective and resonant coupling [see Fig. 2(b)], to implement nontrivial two-qubit gates. The considered interaction

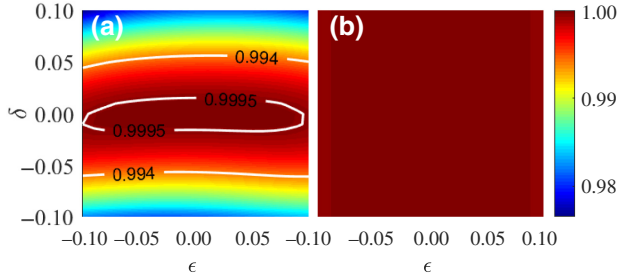


FIG. 5. The gate robustness of the  $S$  gate in DCNHQC (a) without and (b) with the DFS encoding, considering both the  $X$  error and the collective  $Z$  error, where the encoded case performs much better.

Hamiltonian is

$$\mathcal{H}_2(t) = g_1(t)e^{-i\varphi_3}S_2^+S_3^- + g_2(t)e^{-i\varphi_4}S_2^+S_4^- + \text{H.c.}, \quad (14)$$

where  $g_k(t)$  ( $k=1,2$ ) are coupling strengths between qubit pairs  $Q_2, Q_3$  and  $Q_2, Q_4$ , respectively. Adhering to the single-qubit DFS encoding, there exists a six-dimensional DFS  $\mathcal{S}_2 = \text{Span}\{|100100\rangle, |100010\rangle, |010100\rangle, |010010\rangle, |110000\rangle, |000110\rangle\}$  with  $|100100\rangle \equiv |1\rangle_1 \otimes |0\rangle_2 \otimes |0\rangle_{A_1} \otimes |1\rangle_3 \otimes |0\rangle_4 \otimes |0\rangle_{A_2}$ , and the logical qubits are defined as  $\{|00\rangle_L = |100100\rangle, |01\rangle_L = |100010\rangle, |10\rangle_L = |010100\rangle, |11\rangle_L = |010010\rangle\}$ , where  $|A_1\rangle_L = |110000\rangle$  and  $|A_2\rangle_L = |000110\rangle$  are two auxiliary states. In this two-qubit DFS subspace, the Hamiltonian of the coupled system in Eq. (14) changes to

$$\begin{aligned} \mathcal{H}_L^2(t) = & g_1(t)e^{-i\varphi_3}|A_1\rangle_L\langle 00| + g_2(t)e^{-i\varphi_4}|A_1\rangle_L\langle 01| \\ & + g_1(t)e^{-i\varphi_3}|11\rangle_L\langle A_2| + g_2(t)e^{-i\varphi_4}|10\rangle_L\langle A_2| \\ & + \text{H.c.}, \end{aligned} \quad (15)$$

which has two three-level structures, in subspaces  $\text{Span}\{|00\rangle_L, |01\rangle_L, |A_1\rangle_L\}$  and  $\text{Span}\{|10\rangle_L, |11\rangle_L, |A_2\rangle_L\}$  [10], each of which has the same form with the Hamiltonian  $\mathcal{H}(t)$  in Eq. (1). Then, we can also implement dynamically corrected nonadiabatic holonomic two-qubit gates, which suppresses both the  $X$  and  $Z$  errors.

Specifically, besides the two inserted Hamiltonians, when  $\int_0^\tau \sqrt{g_1(t)^2 + g_2(t)^2} dt = \pi$  and the geometric phase is  $\pi$ , the evolution operator in subspaces  $\text{Span}\{|00\rangle_L, |01\rangle_L, |A_1\rangle_L, |10\rangle_L, |11\rangle_L, |A_2\rangle_L\}$  for the Hamiltonian in Eq. (15) can be written as

$$U_T(\eta, \varphi) = \begin{pmatrix} \cos \eta & \sin \eta e^{-i\varphi} & 0 & 0 & 0 & 0 \\ \sin \eta e^{i\varphi} & -\cos \eta & 0 & 0 & 0 & 0 \\ 0 & 0 & -i & 0 & 0 & 0 \\ 0 & 0 & 0 & -\cos \eta & \sin \eta e^{-i\varphi} & 0 \\ 0 & 0 & 0 & \sin \eta e^{i\varphi} & \cos \eta & 0 \\ 0 & 0 & 0 & 0 & 0 & -i \end{pmatrix}, \quad (16)$$

where  $\tan(\eta/2) = g_1(t)/g_2(t)$ , with  $\eta$  being a constant angle and  $\varphi = \varphi_3 - \varphi_4 + \pi$ . Notably, there are no transitions between the two-logical-qubit subspace  $\text{Span}\{|00\rangle_L, |01\rangle_L, |10\rangle_L, |11\rangle_L\}$  and the auxiliary subspace  $\text{Span}\{|A_1\rangle_L, |A_2\rangle_L\}$ ; thus, the evolution operator in the two-logical-qubit subspace reduces to [10]

$$U_2(\eta, \varphi) = \begin{pmatrix} \cos \eta & \sin \eta e^{-i\varphi} & 0 & 0 \\ \sin \eta e^{i\varphi} & -\cos \eta & 0 & 0 \\ 0 & 0 & -\cos \eta & \sin \eta e^{-i\varphi} \\ 0 & 0 & \sin \eta e^{i\varphi} & \cos \eta \end{pmatrix}. \quad (17)$$

Notably, the operations in two subspaces of  $\{|00\rangle_L, |01\rangle_L\}$  and  $\{|10\rangle_L, |11\rangle_L\}$  are different; thus the operator in Eq. (17) denotes a nontrivial two-qubit gate in general. For example,  $U_2(\pi/4, 0) \equiv C$  is an entangling gate [38], and

$$\begin{aligned} C \times (I_1 \otimes H_2) &= \begin{pmatrix} 1 & 0 & 0 & 0 \\ 0 & 1 & 0 & 0 \\ 0 & 0 & 0 & -1 \\ 0 & 0 & 1 & 0 \end{pmatrix} \\ &= \text{CNOT} \times \text{CP}, \end{aligned} \quad (18)$$

where CP is the controlled-phase gate. Furthermore, when  $\Gamma = 2 \times 10^{-4}$ , as shown in Fig. 6, we simulate the state dynamics of gate  $C$  governed by Eq. (14), with an initial product state of  $(|0\rangle_L + |1\rangle_L)|0\rangle_L/\sqrt{2}$  and a state fidelity of  $F_C = 99.82\%$ . In this case, the corresponding final state is

$$\begin{aligned} & (|00\rangle_L + |01\rangle_L - |10\rangle_L + |11\rangle_L)/2 \\ & = (|-0\rangle_L + |+1\rangle_L)/\sqrt{2}, \end{aligned}$$

where  $|\pm\rangle = (|0\rangle_L \pm |1\rangle_L)/\sqrt{2}$ , which is an entangled state. As our manipulation of the logical-qubit subspace only involves the single-excitation subspace of the governed Hamiltonian in Eqs. (12) and (14), the physical-qubit leakage and other high-order oscillating terms can be effectively suppressed, which leads to negligible gate infidelity. Meanwhile, due to the DFS encoding, the dephasing-induced gate infidelity is also negligible, less than 0.01%. Thus, the gate infidelity here, about 0.18%, is mainly due to the qubit-decay effect, which can be further suppressed by improving the lifetime of the physical qubit or shortening the gate time.

## V. CONCLUSION

In conclusion, we propose a general scheme for universal NHQC with the dynamical-correction technique, which can improve gate robustness against the  $X$  error from the second order of the conventional NHQC case to the fourth order, thus retaining the main merit of geometric quantum gates. Numerical simulation shows that our

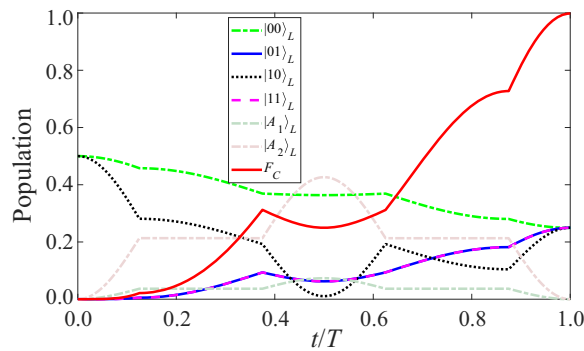


FIG. 6. The state dynamics of gate  $C$  for an initial state of  $(|0\rangle_L + |1\rangle_L)|0\rangle_L/\sqrt{2}$ .

current protocol can be better than previous implementations. Remarkably, when incorporating a DFS encoding, our scheme can also be robust against the  $Z$  errors. Finally, we present the physical implementation of the dynamically corrected protocol with DFS encoding using exchange interactions, which is a thoroughly conventional approach in solid-state quantum systems. Therefore, our scheme provides a promising strategy for future scalable fault-tolerant quantum computation.

### ACKNOWLEDGMENTS

This work was supported by the Key-Area Research and Development Program of Guangdong Province (Grant No. 2018B030326001), the National Natural Science Foundation of China (Grant No. 11874156), and the Science and Technology Program of Guangzhou (Grant No. 2019050001).

[1] P. W. Shor, in *Proceedings of the 35th Annual Symposium on the Foundations of Computer Science* (IEEE Press, Los Alamitos, California, 1994).

[2] F. Arute, K. Arya, R. Babbush, D. Bacon, J. C. Bardin, R. Barends, R. Biswas, S. Boixo, F. G. S. L. Brandao, and D. A. Buell *et al.*, Quantum supremacy using a programmable superconducting processor, *Nature (London)* **574**, 505 (2019).

[3] M. V. Berry, Quantal phase factors accompanying adiabatic changes, *Proc. R. Soc. London A* **392**, 45 (1984).

[4] F. Wilczek and A. Zee, Appearance of Gauge Structure in Simple Dynamical Systems, *Phys. Rev. Lett.* **52**, 2111 (1984).

[5] Y. Aharonov and J. Anandan, Phase Change during a Cyclic Quantum Evolution, *Phys. Rev. Lett.* **58**, 1593 (1987).

[6] P. Zanardi and M. Rasetti, Holonomic quantum computation, *Phys. Lett. A* **264**, 94 (1999).

[7] J. Pachos, P. Zanardi, and M. Rasetti, Non-Abelian Berry connections for quantum computation, *Phys. Rev. A* **61**, 010305(R) (1999).

[8] L.-M. Duan, J. I. Cirac, and P. Zoller, Geometric manipulation of trapped ions for quantum computation, *Science* **292**, 1695 (2001).

[9] L. X. Cen, X. Q. Li, Y. J. Yan, H. Z. Zheng, and S. J. Wang, Evaluation of Holonomic Quantum Computation: Adiabatic versus Nonadiabatic, *Phys. Rev. Lett.* **90**, 147902 (2003).

[10] E. Sjöqvist, D. M. Tong, L. M. Andersson, B. Hessmo, M. Johansson, and K. Singh, Non-adiabatic holonomic quantum computation, *New J. Phys.* **14**, 103035 (2012).

[11] G. F. Xu, J. Zhang, D. M. Tong, E. Sjöqvist, and L. C. Kwek, Nonadiabatic Holonomic Quantum Computation in Decoherence-Free Subspaces, *Phys. Rev. Lett.* **109**, 170501 (2012).

[12] Y.-C. Zheng and T. A. Brun, Fault-tolerant holonomic quantum computation in surface codes, *Phys. Rev. A* **91**, 022302 (2015).

[13] G. F. Xu, C. L. Liu, P. Z. Zhao, and D. M. Tong, Nonadiabatic holonomic gates realized by a single-shot implementation, *Phys. Rev. A* **92**, 052302 (2015).

[14] E. Herterich and E. Sjöqvist, Single-loop multiple-pulse nonadiabatic holonomic quantum gates, *Phys. Rev. A* **94**, 052310 (2016).

[15] Z.-P. Hong, B.-J. Liu, J.-Q. Cai, X.-D. Zhang, Y. Hu, Z. D. Wang, and Z.-Y. Xue, Implementing universal nonadiabatic holonomic quantum gates with transmons, *Phys. Rev. A* **97**, 022332 (2018).

[16] B.-J. Liu, Z.-H. Huang, Z.-Y. Xue, and X.-D. Zhang, Superadiabatic holonomic quantum computation in cavity QED, *Phys. Rev. A* **95**, 062308 (2017).

[17] J. Zhang, S. J. Devitt, J. Q. You, and F. Nori, Holonomic surface codes for fault-tolerant quantum computation, *Phys. Rev. A* **97**, 022335 (2018).

[18] N. Ramberg and E. Sjöqvist, Environment-Assisted Holonomic Quantum Maps, *Phys. Rev. Lett.* **122**, 140501 (2019).

[19] C. Wu, Y. Wang, X.-L. Feng, and J.-L. Chen, Holonomic Quantum Computation in Surface Codes, *Phys. Rev. Appl.* **13**, 014055 (2020).

[20] P. Z. Zhao, K. Z. Li, G. F. Xu, and D. M. Tong, General approach for constructing Hamiltonians for nonadiabatic holonomic quantum computation, *Phys. Rev. A* **101**, 062306 (2020).

[21] B.-J. Liu and M.-H. Yung, Leakage Suppression for Holonomic Quantum Gates, *Phys. Rev. Appl.* **14**, 034003 (2020).

[22] A. Abdumalikov, J. M. Fink, K. Juliusson, M. Pechal, S. Berger, A. Wallraff, and S. Filipp, Experimental realization of non-Abelian non-adiabatic geometric gates, *Nature (London)* **496**, 482 (2013).

[23] G. Feng, G. Xu, and G. Long, Experimental Realization of Nonadiabatic Holonomic Quantum Computation, *Phys. Rev. Lett.* **110**, 190501 (2013).

[24] C. Zu, W.-B. Wang, L. He, W.-G. Zhang, C.-Y. Dai, F. Wang, and L.-M. Duan, Experimental realization of universal geometric quantum gates with solid-state spins, *Nature (London)* **514**, 72 (2014).

[25] S. Arroyo-Camejo, A. Lazariev, S. W. Hell, and G. Balasubramanian, Room temperature high-fidelity holonomic single-qubit gate on a solid-state spin, *Nat. Commun.* **5**, 4870 (2014).

- [26] Y. Sekiguchi, N. Niikura, R. Kuroiwa, H. Kano, and H. Kosaka, Optical holonomic single quantum gates with a geometric spin under a zero field, *Nat. Photonics* **11**, 309 (2017).
- [27] B. B. Zhou, P. C. Jerger, V. O. Shkolnikov, F. J. Heremans, G. Burkard, and D. D. Awschalom, Holonomic Quantum Control by Coherent Optical Excitation in Diamond, *Phys. Rev. Lett.* **119**, 140503 (2017).
- [28] H. Li, L. Yang, and G. Long, Experimental realization of single-shot nonadiabatic holonomic gates in nuclear spins, *Sci. China: Phys., Mech. Astron.* **60**, 080311 (2017).
- [29] Y. Xu, W. Cai, Y. Ma, X. Mu, L. Hu, T. Chen, H. Wang, Y. P. Song, Z.-Y. Xue, Z.-Q. Yin, and L. Sun, Single-Loop Realization of Arbitrary Nonadiabatic Holonomic Single-Qubit Quantum Gates in a Superconducting Circuit, *Phys. Rev. Lett.* **121**, 110501 (2018).
- [30] S. B. Zheng, C. P. Yang, and F. Nori, Comparison of the sensitivity to systematic errors between nonadiabatic non-Abelian geometric gates and their dynamical counterparts, *Phys. Rev. A* **93**, 032313 (2016).
- [31] J. Jing, C.-H. Lam, and L.-A. Wu, Non-Abelian holonomic transformation in the presence of classical noise, *Phys. Rev. A* **95**, 012334 (2017).
- [32] Y.-C. Zheng and T. A. Brun, Fault-tolerant scheme of holonomic quantum computation on stabilizer codes with robustness to low-weight thermal noise, *Phys. Rev. A* **89**, 032317 (2014).
- [33] J. Zhang, L.-C. Kwek, E. Sjöqvist, D. M. Tong, and P. Zanardi, Quantum computation in noiseless subsystems with fast non-Abelian holonomies, *Phys. Rev. A* **89**, 042302 (2014).
- [34] Z.-T. Liang, Y.-X. Du, W. Huang, Z.-Y. Xue, and H. Yan, Nonadiabatic holonomic quantum computation in decoherence-free subspaces with trapped ions, *Phys. Rev. A* **89**, 062312 (2014).
- [35] J. Zhou, W.-C. Yu, Y.-M. Gao, and Z.-Y. Xue, Cavity QED implementation of non-adiabatic holonomies for universal quantum gates in decoherence-free subspaces with nitrogen-vacancy centers, *Opt. Express* **23**, 14027 (2015).
- [36] Z.-Y. Xue, J. Zhou, and Z. D. Wang, Universal holonomic quantum gates in decoherence-free subspace on superconducting circuits, *Phys. Rev. A* **92**, 022320 (2015).
- [37] Y. Wang, J. Zhang, C. Wu, J. Q. You, and G. Romero, Holonomic quantum computation in the ultrastrong-coupling regime of circuit QED, *Phys. Rev. A* **94**, 012328 (2016).
- [38] Z.-Y. Xue, J. Zhou, Y.-M. Chu, and Y. Hu, Nonadiabatic holonomic quantum computation with all-resonant control, *Phys. Rev. A* **94**, 022331 (2016).
- [39] Z.-Y. Xue, F.-L. Gu, Z.-P. Hong, Z.-H. Yang, D.-W. Zhang, Y. Hu, and J. Q. You, Nonadiabatic Holonomic Quantum Computation with Dressed-State Qubits, *Phys. Rev. Appl.* **7**, 054022 (2017).
- [40] P. Z. Zhao, G. F. Xu, Q. M. Ding, E. Sjöqvist, and D. M. Tong, Single-shot realization of nonadiabatic holonomic quantum gates in decoherence-free subspaces, *Phys. Rev. A* **95**, 062310 (2017).
- [41] L.-N. Ji, T. Chen, and Z.-Y. Xue, Scalable nonadiabatic holonomic quantum computation on a superconducting qubit lattice, *Phys. Rev. A* **100**, 062312 (2019).
- [42] Y. Wang, Y. Su, X. Chen, and C. Wu, Dephasing-Protected Scalable Holonomic Quantum Computation on a Rabi Lattice, *Phys. Rev. Appl.* **14**, 044043 (2020).
- [43] G. F. Xu, P. Z. Zhao, T. H. Xing, E. Sjöqvist, and D. M. Tong, Composite nonadiabatic holonomic quantum computation, *Phys. Rev. A* **95**, 032311 (2017).
- [44] Z. Zhu, T. Chen, X. Yang, J. Bian, Z.-Y. Xue, and X. Peng, Single-Loop and Composite-Loop Realization of Nonadiabatic Holonomic Quantum Gates in a Decoherence-Free Subspace, *Phys. Rev. Appl.* **12**, 024024 (2019).
- [45] Y. Sekiguchi, Y. Komura, and H. Kosaka, Dynamical Decoupling of a Geometric Qubit, *Phys. Rev. Appl.* **12**, 051001 (2019).
- [46] X. Wu and P. Z. Zhao, Universal nonadiabatic geometric gates protected by dynamical decoupling, *Phys. Rev. A* **102**, 032627 (2020).
- [47] B.-J. Liu, X.-K. Song, Z.-Y. Xue, X. Wang, M.-H. Yung, Plug-and-Play Approach to Nonadiabatic Geometric Quantum Gates, *Phys. Rev. Lett.* **123**, 100501 (2019).
- [48] T. Yan, B.-J. Liu, K. Xu, C. Song, S. Liu, Z. Zhang, H. Deng, Z. Yan, H. Rong, K. Huang, M.-H. Yung, Y. Chen, and D. Yu, Experimental Realization of Nonadiabatic Shortcut to Non-Abelian Geometric Gates, *Phys. Rev. Lett.* **122**, 080501 (2019).
- [49] S. Li, T. Chen, and Z.-Y. Xue, Fast holonomic quantum computation on superconducting circuits with optimal control, *Adv. Quantum Technol.* **3**, 2000001 (2020).
- [50] M.-Z. Ai, S. Li, Z. Hou, R. He, Z.H. Qian, Z.-Y. Xue, J.-M. Cui, Y.-F. Huang, C.-F. Li, and G.-C. Guo, Experimental Realization of Nonadiabatic Holonomic Single-Qubit Quantum Gates with Optimal Control in a Trapped Ion, *Phys. Rev. Appl.* **14**, 054062 (2020).
- [51] M.-Z. Ai, R. He, S. Li, Z.-Y. Xue, J.-M. Cui, Y.-F. Huang, C.-F. Li, and G.-C. Guo, Experimental Realization of Nonadiabatic Holonomic Single-Qubit Quantum Gates with Two Dark Paths in a Trapped Ion, [arXiv:2101.07483](https://arxiv.org/abs/2101.07483).
- [52] B.-J. Liu, Y.-S. Wang, and M.-H. Yung, Global Property Condition-Based Non-Adiabatic Geometric Quantum Control, [arXiv:2008.02176](https://arxiv.org/abs/2008.02176).
- [53] G. F. Xu, D. M. Tong, and E. Sjöqvist, Path-shortening realizations of nonadiabatic holonomic gates, *Phys. Rev. A* **98**, 052315 (2018).
- [54] F. Zhang, J. Zhang, P. Gao, and G. Long, Searching nonadiabatic holonomic quantum gates via an optimization algorithm, *Phys. Rev. A* **100**, 012329 (2019).
- [55] T. Chen, P. Shen, and Z.-Y. Xue, Robust and Fast Holonomic Quantum Gates with Encoding on Superconducting Circuits, *Phys. Rev. Appl.* **14**, 034038 (2020).
- [56] B.-J. Liu, Z.-Y. Xue, M.-H. Yung, Brachistochronic Non-Adiabatic Holonomic Quantum Control, [arXiv:2001.05182](https://arxiv.org/abs/2001.05182).
- [57] Z. Han, Y. Dong, B. Liu, X. Yang, S. Song, L. Qiu, D. Li, J. Chu, W. Zheng, J. Xu, T. Huang, Z. Wang, X. Yu, X. Tan, D. Lan, M.-H. Yung, and Y. Yu, Experimental Realization of Universal Time-Optimal Non-Abelian Geometric Gates, [arXiv:2004.10364](https://arxiv.org/abs/2004.10364).
- [58] K. Khodjasteh and L. Viola, Dynamically Error-Corrected Gates for Universal Quantum Computation, *Phys. Rev. Lett.* **102**, 080501 (2009).



- [59] X. Wang, L. S. Bishop, J. P. Kestner, E. Barnes, K. Sun, and S. D. Sarma, Composite pulses for robust universal control of singlet-triplet qubits, *Nat. Commun.* **3**, 997 (2012).
- [60] X. Rong, J. Geng, F. Shi, Y. Liu, K. Xu, W. Ma, F. Kong, Z. Jiang, Y. Wu, and J. Du, Experimental fault-tolerant universal quantum gates with solid-state spins under ambient conditions, *Nat. Commun.* **6**, 8748 (2015).
- [61] L.-M. Duan and G.-C. Guo, Preserving Coherence in Quantum Computation by Pairing Quantum Bits, *Phys. Rev. Lett.* **79**, 1953 (1997).
- [62] P. Zanardi and M. Rasetti, Noiseless Quantum Codes, *Phys. Rev. Lett.* **79**, 3306 (1997).
- [63] D. A. Lidar, I. L. Chuang, and K. B. Whaley, Decoherence-Free Subspaces for Quantum Computation, *Phys. Rev. Lett.* **81**, 2594 (1998).
- [64] P. Shen, T. Chen, and Z.-Y. Xue, Ultrafast Holonomic Quantum Gates, *Phys. Rev. Appl.* **16**, 044004 (2021).
- [65] M. H. Devoret and R. J. Schoelkopf, Superconducting circuits for quantum information: An outlook, *Science* **339**, 1169 (2013).
- [66] A. Klappenecker and M. Rotteler, Mutually unbiased bases are complex projective 2-designs, *Proc. Int. Symp. Inf. Theory* **2005**, 1740 (2005).